Check for updates

Preparation of magnetic carbon/Fe_3O_4 supported zero-valent iron composites and their application in Pb(II) removal from aqueous solutions

Kaixuan Ma, Qiu Wang, Qianyun Rong, Dapeng Zhang, Shihai Cui and Jing Yang

ABSTRACT

Nanoscale zero-valent iron (NZVI) was first assembled on magnetic carbon/Fe_3O_4 (CM) with a combination of hydrothermal and liquid phase reduction methods. The novel NZVI@CM magnetic nanocomposites have the merits of large surface area, unique magnetic property, low cost and environmental friendliness. They can be used for Pb(II) removal in aqueous solution. The materials were characterized by using transmission electron microscopy (TEM), X-ray diffraction (XRD), Fourier transform-infrared spectroscopy (FT-IR), thermogravimetric analysis (TGA), vibrating sample magnetometry (VSM), X-ray photoelectron spectroscopy (XPS) and Brunauer–Emmett–Teller (BET) adsorption. The various parameters, such as reaction time, dosage of catalyst, solution pH and acid ions concentrations were studied. The removal efficiency of Pb(II) can be obviously increased by the combination of appropriate CM and NZVI. The removal efficiency of Pb(II) is 99.7% by using 60 mg of NZVI@CM at pH 7. The kinetics study indicates that the Pb(II) removal accords to pseudo-second-order kinetics model.

Key words | carbon/Fe_3O_4, magnetic materials, nanocomposites, nanoscale-zerovalent-iron, Pb(II) removal

Kaixuan Ma
Qiu Wang
Qianyun Rong
Dapeng Zhang
Shihai Cui (corresponding author)
Jing Yang
Jiangsu Collaborative Innovation Center of Biomedical Functional Materials, Jiangsu Key Laboratory of Biomedical Materials, College of Chemistry and Materials Science, Jiangsu Provincial Key Laboratory of Materials Cycling and Pollution Control,
Nanjing Normal University,
1 Wenyuan Road,
Nanjing 210023,
China
E-mail: *cuishihai@njnu.edu.cn*

Dapeng Zhang
Shihai Cui
Nanjing Lvshiyuan Environmental Protection Technology Co., Ltd,
108 Ganjiabiandong Road,
Nanjing 210033,
China

INTRODUCTION

Heavy metals have been widely used in industrial areas such as painting pigments, storage batteries manufacturing, fuels, explosives manufacturing, photographic materials, automobiles, coatings, aeronautical, and metallurgical (steel) (Arshadi *et al.* 2014). However, heavy metal ions are one of the most toxic inorganic pollutants in the environment, especially in water systems, and arouse crucial concerns. Pb(II) is a common heavy metal ion. It can cause serious damages to bone, muscle, kidney, nervous system, and the brain (Xi *et al.* 2010; Zhang *et al.* 2010; He *et al.* 2014). The industry of lead mining, smelting, and consuming can always produce lead pollution. It has been reported that over 20 million tons of wastewater containing Pb(II) was generated each year (Liu *et al.* 2015). Therefore, the effective recovery of Pb(II) from wastewater has been a crucial issue related to the quality of human life and ecological environment (Zhang *et al.* 2013).

Many different methods have been applied to treat heavy metal polluted wastewater, including membrane separation, chemical precipitation, adsorption, and ion-exchange (Fu & Wang 2011; Hua *et al.* 2012; Vijayaraghavan & Joshi 2013; Liu *et al.* 2015). In recent years, nanoscale zero-valent iron (NZVI) has become one of the most widely used materials in pollutants removal. It has received extensive attentions because of its simple synthesis method, large specific surface area, high reaction activity, and strong reductive power (Crane & Scott 2012; Yan *et al.* 2013; Arancibia-Miranda *et al.* 2014). There are many reports about the application of NZVI in removing various pollutants, such as nitrates (Cho *et al.* 2015), C.I. acid orange 7 (Yuan *et al.* 2014), chlorinated organic compounds (Hwang *et al.* 2015), and heavy metal ions (Zhang *et al.* 2010, 2011, 2014; Sun *et al.* 2014). However, NZVI has a tendency to aggregate because of its natural predisposition to remain in a more thermodynamically stable state (Mackenzie *et al.* 2012; Xu *et al.* 2014). Various modification methods have been adopted to improve the performance of catalytic

doi: 10.2166/wst.2017.384

Downloaded from http://iwaponline.com/wst/article-pdf/76/10/2680/241237/wst076102680.pdf
by guest

materials. The preparation of bimetallic composite materials is one of the modification methods. For example, Han *et al.* (Han *et al.* 2016) prepared a mixed NZVI and zero-valent aluminum catalyst to remove heavy metals and achieved a high efficiency. Incorporating NZVI particles onto some support materials can also successfully reduce the aggregation of NZVI particles and improve their performance in pollutant treatment. The frequently used supports are kaolin (Zhang *et al.* 2010, 2011), $Mg(OH)_2$ (Liu *et al.* 2015), S-NaOH (Arshadi *et al.* 2014), zeolite (Kim *et al.* 2013), carbon (Mackenzie *et al.* 2012; Xu *et al.* 2014), and graphene (Jabeen *et al.* 2013).

Fe_3O_4 nanoparticle is a useful material that has received increasing attention. It has good physical and chemical properties, including unique magnetic properties, easiness to functional modification, high separation efficiency, and environmental friendliness. It is often used in the synthesis of catalytic materials (Zhang *et al.* 2013; Lv *et al.* 2014; Akhundi & Habibi-Yangjeh 2015; Shi *et al.* 2015; Yang *et al.* 2016). In order to obtain high stability, dispersibility, and separability, Fe_3O_4 nanoparticle can be introduced in combination with NZVI.

In this study, carbon/Fe_3O_4 supported zero-valent iron composites (NZVI@CM) were prepared by hydrothermal and liquid-phase reduction methods. The composites were characterized by transmission electron microscopy (TEM), X-ray diffraction (XRD), Fourier transform-infrared spectroscopy (FT-IR), thermogravimetric analysis (TGA), vibrating sample magnetometry (VSM), X-ray photoelectron spectroscopy (XPS) and Brunauer–Emmett–Teller (BET) adsorption. The ability of NZVI@CM magnetic nanocomposites to remove Pb(II) from aqueous solution was investigated. The various reaction conditions were optimized for Pb(II) removal. A kinetic study was also carried out in this study.

EXPERIMENTAL

Materials

Lead acetate, ferric chloride hexahydrate, sodium borohydride, anhydrous ethylene glycol, sodium acetate anhydrous, glucose, sodium chloride, sodium nitrate, sodium hydroxide and sulfuric acid (analytical reagent) were obtained from Sinopharm Chemical Reagent Company (Shanghai, China). All chemicals were used without any further purification. Purified water (Wahaha Group Ltd, Hangzhou, China) was used throughout the experiments.

Apparatus

Transmission electron micrographs (TEM) were taken by a JEM-200CX (JEOL, Tokyo, Japan) microscope operating at a 200 kV accelerating voltage. XRD patterns were recorded by a Rigaku D/max 2500/PC instrument. FT-IR spectra were recorded over 4,000 – 400 cm^{-1} in a Tensor 27 spectrometer (Bruker, Germany). Thermogravimetric measurements were performed on a STA 449 F3 Jupiter simultaneous thermal analyzer at a heating rate of 10°C min^{-1} in nitrogen (Netzsth, Selb, Germany). The magnetism measurement of the nanomaterials was examined using a VSM (Quantum Design, San Diego, CA, USA) at room temperature. XPS analysis was performed on a PHI 5000 VersaProbe system, using monochromatic Al Kα radiation (1,486.6 eV) operating at an accelerating power of 15 kW (UlVAC-PHI, Kanagawa, Japan). BET surface area analysis was performed using nitrogen adsorption method with an ASAP2020 surface analyzer (Micromeritics Instrument, USA). The concentration of Pb(II) was analyzed by atomic absorption spectrometer (AAS) using AVANTA (GBC, Australia) by 283.3 nm.

Preparation of the NZVI@CM nanocomposites

Preparation of Fe_3O_4 magnetic nanoparticles

Fe_3O_4 nanoparticles were synthesized by solvothermal method on the basis of our preceding work (Yang *et al.* 2016) with minor modifications. Briefly, 1.35 g $FeCl_3{\cdot}6H_2O$ was added to 40 mL anhydrous ethylene glycol with magnetic stirring. Then 3.6 g sodium acetate anhydrous was added to the mixture. After 30 min stirring, the solution was transferred to a Teflon-sealed autoclave and heated at 198°C. After reaction for 6 h, the autoclave was cooled to room temperature. The products were washed with water and anhydrous ethanol several times, respectively.

Preparation of CM magnetic nanocomposites

The Fe_3O_4 synthesized above was dispersed in 0.5 mol·L^{-1} glucose solution. After ultrasonic mixing for 30 min, the mixed solution was transferred to a Teflon-sealed autoclave at 180°C for 4 h. Then the products CM were washed with water and anhydrous ethanol several times, alternately.

Preparation of NZVI@CM magnetic nanocomposites

Here, 0.2 g CM magnetic nanocomposites were transferred into a three-necked flask, 20 mL $Fe(OH)_3$ colloid and

Downloaded from http://iwaponline.com/wst/article-pdf/76/10/2680/241237/wst076102680.pdf
by guest

20 mL absolute ethyl alcohol were poured into this flask under vigorous stirring. Finally, 10 mL 25 $g \cdot L^{-1}$ $NaBH_4$ solution was added to the flask under N_2 protection by the rate of 2 drops per second. After 15 min reduction, magnetic nanoparticles were collected by magnet and washed with water. The products NZVI@CM were stored in anhydrous ethanol to reduce oxidization. NZVI was synthesized by the same method above without the addition of CM particles.

The removal experiments of Pb(II)

The pH of Pb(II) aqueous solution was adjusted to 7.0 with the acetic acid-ammonium acetate buffer solution. In an oxygen limited condition, a certain NZVI@CM magnetic nanocomposites were added to 40 mL 500 $mg \cdot L^{-1}$ Pb(II) solutions at 25°C in water-bathing. Aliquots of samples were taken at certain time intervals, and filtered immediately through 0.45 μm filter membranes. The concentrations of the Pb(II) aqueous solution were analyzed in AAS. The degradation percentage was obtained using Equation (1) as follows:

$$\text{Degradation percentage} = \left[\frac{(C_0 - C)}{C_0}\right] \times 100\% \quad (1)$$

where C_0 is the initial concentration of Pb(II) aqueous solution (units: $mg \cdot L^{-1}$) and C is the concentration of Pb(II) aqueous solution after the degradation (units: $mg \cdot L^{-1}$).

RESULTS AND DISCUSSION

Characterization of NZVI@CM magnetic nanocomposites

TEM analysis

Figure 1 shows the TEM images of Fe_3O_4, CM, NZVI, and NZVI@CM magnetic nanomaterials. The TEM image of the Fe_3O_4 magnetic particles (Figure 1(a)) exhibits a monodispersed spherical structure with an average diameter of approximately 100–150 nm. The CM magnetic

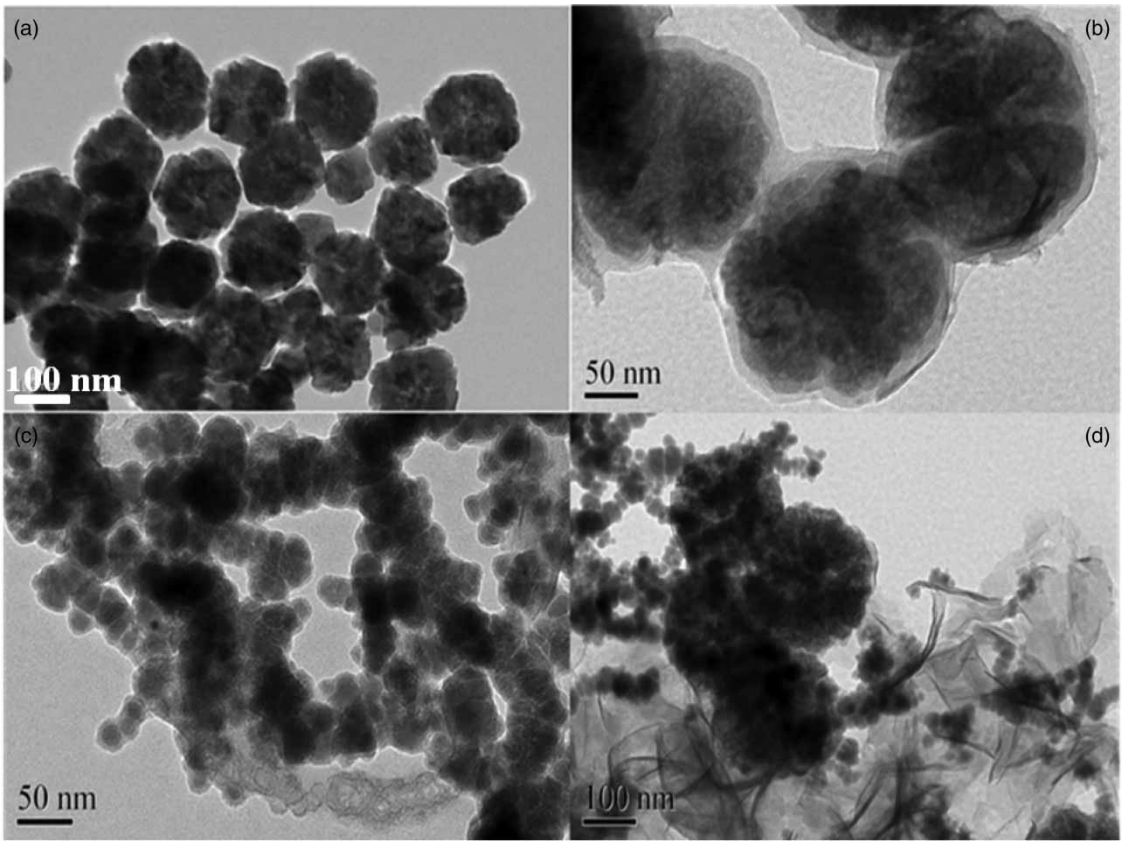

Figure 1 | TEM images of (a) Fe_3O_4, (b) CM, (c) NZVI and (d) NZVI@CM.

Downloaded from http://iwaponline.com/wst/article-pdf/76/10/2680/241237/wst076102680.pdf
by guest

nanocomposites (Figure 1(b)) show the formation of a spherical carbon layer on the surface of the Fe_3O_4 magnetic nanoparticles. This demonstrates that the surface of the Fe_3O_4 was covered by a carbon layer. NZVI particles (Figure 1(c)) have average diameters of approximately 20–25 nm. The NZVI has a chain-like shape and aggregated structure because it tends to remain in a more thermodynamically stable state (Mackenzie *et al.* 2012; Xu *et al.* 2014). The NZVI@CM magnetic nanocomposites (Figure 1(d)) show that the NZVI particles were assembled and dispersed on the surface of the CM magnetic nanocomposites.

XRD analysis

Figure 2 shows the XRD patterns of the Fe_3O_4, CM, NZVI, and NZVI@CM magnetic nanomaterials. The main XRD angle (2θ) values of the Fe_3O_4 magnetic nanoparticles are 18.2°, 30.1°, 35.5°, 43.0°, 53.5°, 57.0°, and 62.5° (Figure 2(a)) (Lv *et al.* 2014; Akhundi & Habibi-Yangjeh 2015). In Figure 2(b), the peaks of the CM magnetic composite are weaker than those of the Fe_3O_4 nanoparticles because of the outer carbon layer. Figure 2(c) shows the Fe^0 (110) diffraction peak at $2\theta = 44.5°$ (Lv *et al.* 2014; Xu *et al.* 2014), which indicates a good crystallinity of the NZVI particles. In the NZVI@CM nanomaterials, there are diffraction peaks corresponding to both NZVI and Fe_3O_4 (Figure 2(d)). According to Scherrer formula $D = k\lambda/\beta\cos\theta$ (k is 0.89, λ is 0.15405 nm, β is half-peak breadth, and θ is diffraction angle), the size of the nanomaterials is consistent with the result of TEM analysis. It can be seen that the NZVI@CM magnetic nanocomposites were successfully synthesized.

FT-IR analysis

FT-IR spectra of the Fe_3O_4, CM, and NZVI@CM magnetic nanomaterials are shown in Figure 3. The intense signal at 591 cm^{-1} in Figure 3(a) is assigned to the Fe-O stretching vibration of Fe_3O_4 (Rao *et al.* 2009; Yang *et al.* 2010). After the introduction of carbon and NZVI, the Fe-O vibrations turn to weaker (Figure 3(b) and 3(c)), which confirms the hybridization of both NZVI and CM magnetic nanocomposites.

TGA analysis

TGA analysis was performed to determine the weight loss of the material over a certain temperature range. Figure 4 shows the TGA curves of the Fe_3O_4, CM, and NZVI@CM magnetic nanomaterials from room temperature to 800°C. There is a small weight-loss between 650 and 700°C, which is attributed to the transformation of Fe_3O_4 to α-Fe_2O_3 (Deng *et al.* 2005) (Figure 4(a)). Figure 4(c) shows that the CM magnetic nanocomposites undergo a significant weight-loss of about 74%, which can be attributed to the decomposition of carbon coated on the surface of the Fe_3O_4 nanoparticles (Shen *et al.* 2016). The NZVI@CM magnetic nanocomposites (Figure 4(b)) have a weight-loss of about 62.5%, which is lower than that of CM because of the addition of NZVI.

VSM analysis

Figure 5 shows the VSM curves of Fe_3O_4, CM and NZVI@CM nanocomposites at room temperature. The

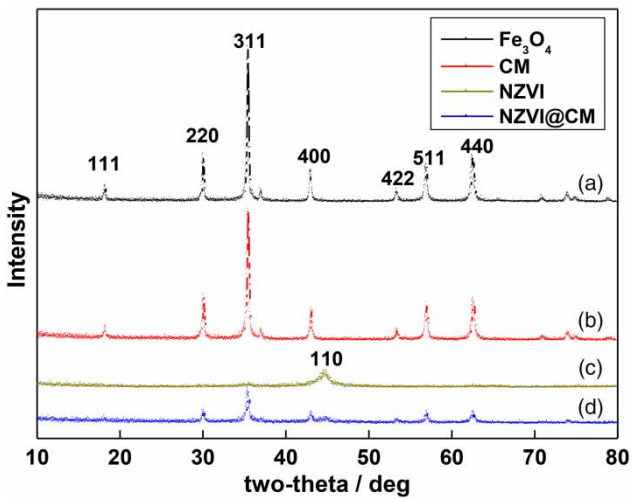

Figure 2 | XRD patterns of (a) Fe_3O_4, (b) CM, (c) NZVI and (d) NZVI@CM.

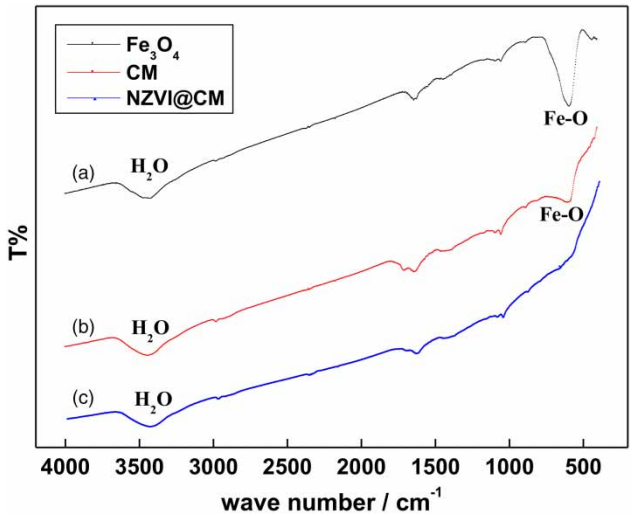

Figure 3 | FT-IR spectrums of (a) Fe_3O_4, (b) CM and (c) NZVI@CM.

Downloaded from http://iwaponline.com/wst/article-pdf/76/10/2680/241237/wst076102680.pdf
by guest

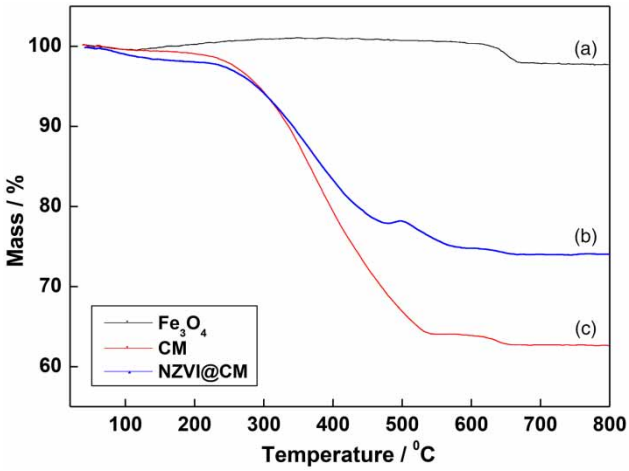

Figure 4 | TGA curves of (a) Fe_3O_4, (b) CM and (c) NZVI@CM.

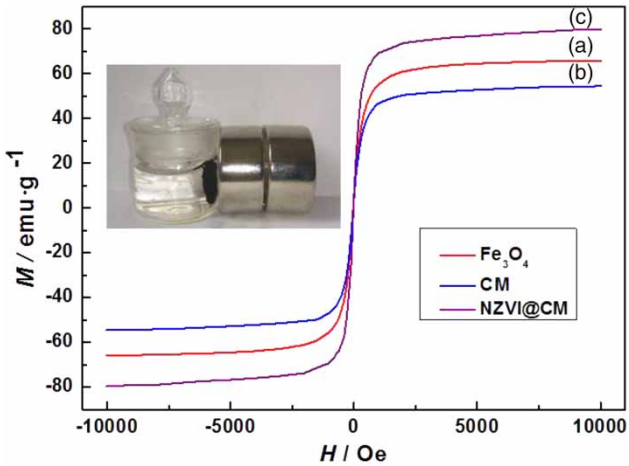

Figure 5 | VSM curves of (a) Fe_3O_4, (b) CM and (c) NZVI@CM.

maximum saturation magnetization of the Fe_3O_4 is 65.86 emu·g^{-1} (Figure 5(a)). The magnetism of the CM nanocomposite is 54.44 emu·g^{-1} (Figure 5(b)), which is smaller than that of Fe_3O_4. It is attributed to the presence of the non-magnetic carbon shell. With the combination of the NZVI and the CM, the magnetism increases and reaches to 79.69 emu·g^{-1} (Figure 5(c)). All of the materials exhibit super paramagnetic behavior. When an external magnetic field was placed under the aqueous solution containing the NZVI@CM nanocomposites, the material can be quickly attracted and separated from the solution, thus preventing the environmental pollution. The photograph of magnetic separation of NZVI@CM in aqueous solution has been provided in the left-top inset of Figure 5.

XPS analysis

The NZVI@CM was further detected by XPS analysis. Figure 6(a) shows the wide scan spectra of NZVI@CM without reaction. The photo electron lines at binding energies of approximately 280, 530 and 710 eV were attributed to C1s, O1s and Fe2p, respectively. Figure 6(b) indicates the electron lines of NZVI@CM after reaction with 500 mg/L Pb(II). There are electron lines of Pb4f. Combined with Figure 6(c), two peaks at the band energy about 136.7 eV and 141.1 eV can be assigned to Pb(0) and Pb(II), respectively (Fu *et al.* 2015). The presence of Pb(II) may be attributed to absorption of the material to Pb(II) solution. The presence of Pb(0) may be ascribed to the reaction with the material. Thus, Fe(0) was oxidized and its electron line at about 704.9 is weaker (Figure 6(d)) (Lv *et al.* 2016; Li *et al.* 2017).

Catalytic degradation of Pb(II)

Effect of the various materials on the removal of Pb(II)

CM, NZVI, and NZVI@CM were used in the experiments of Pb(II) removal, respectively. Different materials show different removal efficiencies. As shown in Figure 7, the decrease of Pb(II) is only 2.09% by using the CM. This may be attributed to the adsorption of Pb(II) on the CM. When the NZVI was applied as the catalyst, the removal rate of Pb(II) increased to 76.8%. This shows a better degradation effect than that obtained with CM. When CM was hybridized with NZVI, the nanocomposite NZVI@CM shows a satisfactory removal rate of 99.7%. It can be seen that NZVI@CM has the best reaction activity. With the introduction of the CM, the NZVI can be dispersed uniformly in the CM. So the NZVI@CM nanocomposite is more stable than the NZVI. The BET N_2 measurement analysis indicates that the surface area of the NZVI@CM was 16.1 m^2/g, which is larger than that of the NZVI (15.0 m^2/g) or CM (6.8 m^2/g). Then more Pb(II) can be adsorbed on the CM, and then removed by the material (Li *et al.* 2006; Üzüm *et al.* 2009; Jiang *et al.* 2010; Zhang *et al.* 2010).

Effect of the amount of NZVI@CM on the Pb(II) removal

In order to determine the optimal amount of NZVI@CM magnetic nanocomposite for Pb(II) removal, various amounts (20, 40, 60 and 80 mg) of NZVI@CM were added into 40 mL of 500 mg·L^{-1} Pb(II) solution. Figure 8 shows the correlation between the catalyst amount and the

Downloaded from http://iwaponline.com/wst/article-pdf/76/10/2680/241237/wst076102680.pdf
by guest

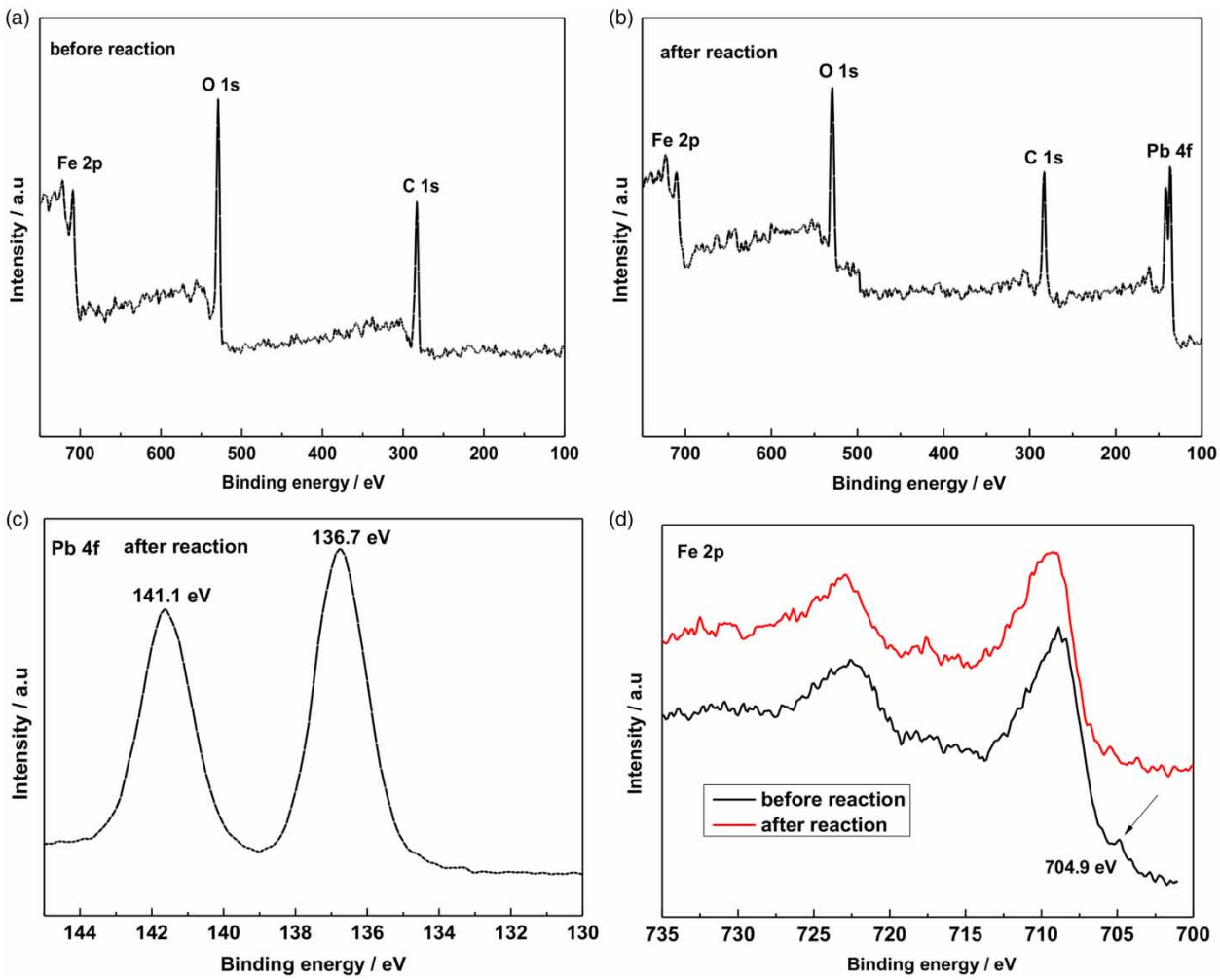

Figure 6 | XPS spectra of wide scan of the NZVI@CM particles before (a) and after (b) reaction with Pb(II); the Pb 4f pattern after reaction (c); the Fe 2p pattern before and after reaction (d).

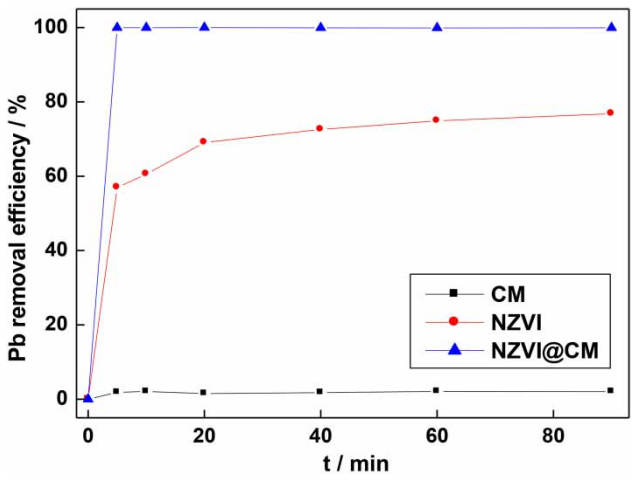

Figure 7 | Pb(II) removal efficiency of CM, NZVI and NZVI@CM (500 mg/L Pb(II), pH = 7.0).

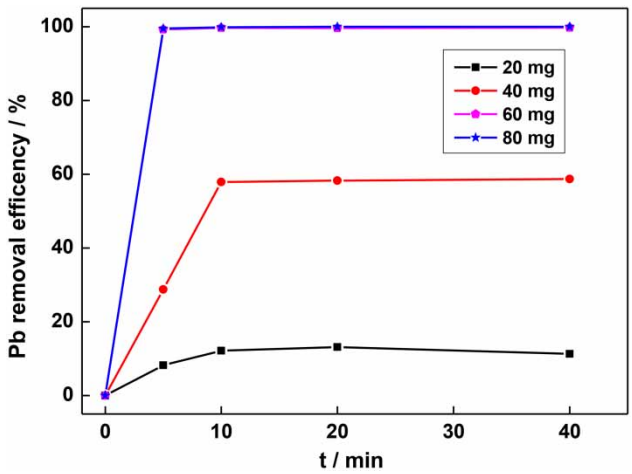

Figure 8 | Pb(II) removal efficiency of different dosages of NZVI@CM (500 mg/L Pb(II), pH = 7.0).

Downloaded from http://iwaponline.com/wst/article-pdf/76/10/2680/241237/wst076102680.pdf
by guest

removal efficiency of Pb(II) by using the NZVI@CM nanocomposite. It can be seen that the removal efficiency of Pb(II) increases with the increase of the catalyst mass due to the higher amount of adsorption sites (Arshadi *et al.* 2014). As the catalyst amount increased from 20 to 60 mg, the removal efficiency of Pb(II) increased from 11.7 to 99.7%. However, adding more NZVI@CM (80 mg) to the Pb(II) aqueous solution did not increase the removal efficiency. At low adsorbent dosages, the active sites on the adsorbent surface are not completely covered and, thus, the removal efficiency increases with the catalyst dosage. At high adsorbent dosages, the active sites on the adsorbent are completely occupied, resulting in a relatively constant removal capacity of Pb(II) from the aqueous solution (Zhang *et al.* 2010). Therefore, 60 mg catalyst dosage was chosen as the optimal amount in the following experiments.

Effect of pH on the Pb(II) removal performance

The pH of the solution is considered one of the most important parameters in the removal process (Xu *et al.* 2014). Figure 9 shows the effect of the initial solution pH on the removal of Pb(II) by using NZVI@CM magnetic nanocomposites. The experiments were carried out in the pH from 3 to 9. It can be seen that when the pH was adjusted from 3 to 7, the maximum removal efficiency increased from 60.3 to 99.7%. When the pH was set to 9, the removal efficiency decreased to 69.1%. When the pH is low, the concentration of H^+ ions is high, which can cause a competition between H^+ ions and Pb(II) for vacant adsorbent sites. Furthermore, H^+ can react with the NZVI, which might lead to a decrease of the Pb(II) removal efficiency. When the pH is high, the concentration of hydroxy ions (OH^-) will increase in solution, which probably result in the precipitation of $Pb(OH)_2$ both in the solution and on the NZVI@CM surface (Katsoyiannis & Zouboulis 2002). The precipitation of $Pb(OH)_2$ may hinder the interaction between the NZVI@CM and Pb(II) and reduces the removal efficiency of Pb(II). So the Pb(II) solution with pH >9.0 was not applied in the condition experiments. The pH 7 was chosen in the following experiments.

Effect of acid ion concentrations on Pb(II) removal

There are numerous ions in wastewater including common acid ions Cl^- and NO_3^-. Figure 10 shows the effects of these two acid ions on the removal efficiency of Pb(II) by using NZVI@CM magnetic nanocomposites. The removal efficiency of Pb(II) decreases gradually with the increase of NO_3^-. This is probably attributed to a redox reaction between NZVI@CM and NO_3^- (Cho *et al.* 2015). The main product of the reaction is NH_4^+, which may cause a large consumption of H^+ and an increase of the alkalinity (Westerhoff & James 2003; Cho *et al.* 2015). The increase of the pH may also decrease the removal efficiency of Pb(II) when using the NZVI@CM nanocomposites.

As the Cl^- concentration increases, the removal efficiency of Pb(II) remains somewhat constant, followed by a slight decrease. When the molar ratio of Cl^- and Pb(II) is lower than or equal to 2, the Cl^- does not influence the removal efficiency of Pb(II). The NZVI@CM can reduce the Pb(II), which is supported by the electrode potentials listed in Equations (2) and (3) (Noubactep 2008; Arancibia-Miranda *et al.* 2014). When the molar ratio of Cl^- and Pb(II)

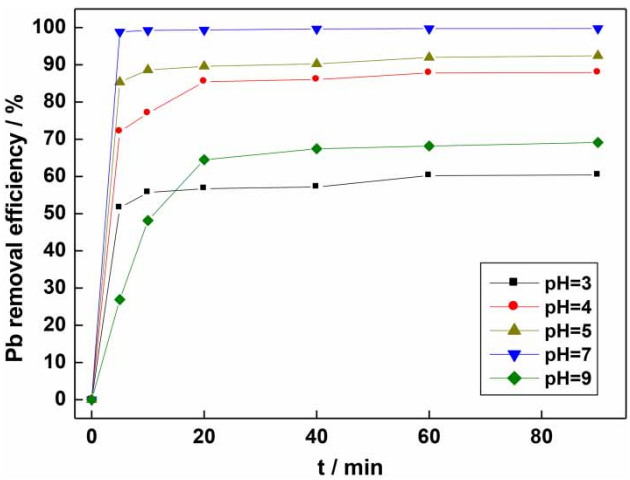

Figure 9 | pH effect on Pb(II) removal performance by NZVI@CM (500 mg/L Pb(II)).

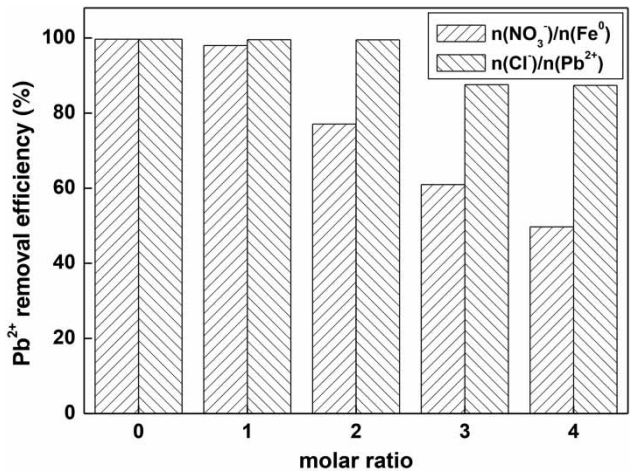

Figure 10 | The effect of Cl^- and NO_3^- on Pb(II) removal performance by NZVI@CM (500 mg/L Pb(II), pH = 7.0).

Downloaded from http://iwaponline.com/wst/article-pdf/76/10/2680/241237/wst076102680.pdf
by guest

is higher than 2, excessive amounts of Cl^- may be combined with the Pb(II) and form $PbCl_3^-$ and $PbCl_4^{2-}$ (Felmy *et al.* 2000). On one hand, the electrode potentials of the coordinates to Pb decreased; on the other hand, the Cl^- around the Pb(II) may prevent the NZVI from removing the Pb (II). Hence, the removal efficiency is decreased.

$$Pb^{2+} + 2e^- = Pb \quad E^\theta = -0.1262 \tag{2}$$

$$Fe^{2+} + 2e^- = Fe \quad E^\theta = -0.4470 \tag{3}$$

Experimental data analysis

Kinetic study of the reaction

In order to determine the rate-determining step, the kinetics of the Pb(II) removal using NZVI@CM were studied. The pseudo-first-order and pseudo-second-order adsorption models are commonly used to determine the reaction kinetics of the Pb(II) removal (Arshadi *et al.* 2014; Lv *et al.* 2014). The kinetic data at different pH were analyzed through the Equations (4)–(6) as follows (Yan *et al.* 2013; Akhundi & Habibi-Yangjeh 2015):

$$\log(q_e - q_t) = \log q_e - \frac{k_1}{2.303}t \tag{4}$$

$$\frac{t}{q_t} = \frac{1}{k_2 q_e^2} + \frac{t}{q_e} \tag{5}$$

$$q_t = (C_0 - C_t) \times \frac{V}{M} \tag{6}$$

where k_1 and k_2 (mg·g^{-1}·min^{-1}) are the pseudo-first-order and pseudo-second-order adsorption rate constants, respectively; q_t and q_e (mg·g^{-1}) are the amounts of Pb(II) adsorbed at time t and at an equilibrium time, respectively; C_0 (mg·L^{-1}) is the initial concentration of Pb(II); C_t (mg·L^{-1}) is the concentrations of Pb(II) at any time t; V (L) is the total volume of the solution; M (g) is the mass of the catalyst. The q_e, k_1, and k_2 values can be calculated through Equations (4) and (5).

Table 1 lists the parameters from the different reaction models. The correlation coefficients (R^2) of the pseudo-second-order kinetic model are all higher than 0.99, while the R^2 of the pseudo-first-order kinetic model are relatively low. The good fitting shows that the pseudo-second-order kinetic model is more suitable for the removal of Pb(II) by using NZVI@CM, which suggests that adsorption might be the rate-determining step of the process. Meanwhile, there is a maximum for k_2 and q_e at pH 7, which leads to the conclusion that pH 7 is the optimal condition. It also conforms to the conclusion of the experiments above. The schematic diagram of the mechanism for the Pb(II) removal by NZVI@CM is shown in Figure 11.

Table 1 | Kinetics parameters for Pb(II) removal by NZVI@CM nanocomposites at different pH

pH	k_1/(min^{-1})	R^2	q_e (mg·g^{-1})
Pseudo-second-order equation			
3	0.0599	0.8169	188.67
4	0.0798	0.9291	275.48
5	0.1479	0.7578	286.53
7	0.0587	0.9900	307.69
9	0.0673	0.8989	229.36
pH	**k_2/(g·mg^{-1}·min^{-1})**	**R^2**	**q_e (mg·g^{-1})**
Pseudo-second-order equation			
3	0.0038	0.9995	188.67
4	0.0029	0.9999	275.48
5	0.0053	0.9999	286.53
7	0.0486	1.0000	307.69
9	0.0008	0.9962	229.36

CONCLUSIONS

In this study, NZVI@CM magnetic nanocomposites were synthesized by using hydrothermal and liquid-phase reduction methods. The structural characterizations were performed by TEM, XRD, FT-IR, TGA, VSM, XPS and BET analysis. It was shown that NZVI was successfully assembled on the surface of CM. This material was used in

Figure 11 | Schematic diagram of the mechanism for the Pb(II) removal by NZVI@CM.

Downloaded from http://iwaponline.com/wst/article-pdf/76/10/2680/241237/wst076102680.pdf
by guest

the Pb(II) removal in aqueous solutions. Different parameters such as reaction time, catalyst loading, solution pH, and acid ion have been discussed and optimized for Pb(II) removal. The results show that the removal efficiency of Pb(II) is 99.7% by using 60 mg of NZVI@CM at pH 7, which is more effective compared to those by using NZVI or CM. The kinetic study indicates that the Pb(II) removal is fitted by a pseudo-second-order kinetic model.

ACKNOWLEDGEMENTS

This work was supported National Natural Science Foundation of China (21177061), Natural Science Foundation of Jiangsu Province (BK20150968) and Technology-Based Pioneering Enterprise Incubation Project of Jiangsu Province (BC2016003).

REFERENCES

Akhundi, A. & Habibi-Yangjeh, A. 2015 Novel magnetically separable g-C_3N_4/AgBr/Fe_3O_4 nanocomposites as visible-light-driven photocatalysts with highly enhanced activities. *Ceram. Int.* **41**, 5634–5643.

Arancibia-Miranda, N., Baltazar, S. E., García, A., Romero, A. H., Rubio, M. A. & Altbir, D. 2014 Lead removal by nano-scale zero valent iron: surface analysis and pH effect. *Mater. Res. Bull.* **59**, 341–348.

Arshadi, M., Soleymanzadeh, M., Salvacion, J. W. & SalimiVahid, F. 2014 Nanoscale Zero-Valent Iron (NZVI) supported on sineguelas waste for Pb(II) removal from aqueous solution: kinetics, thermodynamic and mechanism. *J. Colloid Interface Sci.* **426**, 241–251.

Cho, D. W., Song, H., Schwartz, F. W., Kim, B. & Jeon, B. H. 2015 The role of magnetite nanoparticles in the reduction of nitrate in groundwater by zero-valent iron. *Chemosphere* **125**, 41–49.

Crane, R. A. & Scott, T. B. 2012 Nanoscale zero-valent iron: future prospects for an emerging water treatment technology. *J. Hazard. Mater.* **211–212**, 112–125.

Deng, H., Li, X. L., Peng, Q., Wang, X., Chen, J. P. & Li, Y. D. 2005 Monodisperse magnetic single-crystal ferrite microspheres. *Angew. Chem. Int. Ed.* **44**, 2782–2785.

Felmy, A. R., Onishi, L. M., Foster, N. S., Rustad, J. R., Rai, D. & Mason, M. J. 2000 An aqueous thermodynamic model for the Pb^{2+}–Na^{+}–K^{+}–Ca^{2+}–Mg^{2+}–H^{+}–Cl^{-}–SO_4^{2-}–H_2O system to high concentration: application to WIPP brines. *Geochim. Cosmochim. Acta* **64** (21), 3615–3628.

Fu, F. & Wang, Q. 2011 Removal of heavy metal ions from wastewaters: a review. *J. Environ. Manage.* **92**, 407–418.

Fu, R., Yang, Y., Xu, Z., Zhang, X., Guo, X. & Bi, D. 2015 The removal of chromium (VI) and lead (II) from groundwater using sepiolite-supported nanoscale zero-valent iron (S-NZVI). *Chemosphere* **138**, 726–734.

Han, W., Fu, F., Cheng, Z., Tang, B. & Wu, S. 2016 Studies on the optimum conditions using acid-washed zero-valent iron/aluminum mixtures in permeable reactive barriers for the removal of different heavy metal ions from wastewater. *J. Hazard. Mater.* **302**, 437–446.

He, J., Lu, Y. & Luo, G. 2014 Ca(II) imprinted chitosan microspheres: An effective and green adsorbent for the removal of Cu(II), Cd(II) and Pb(II) from aqueous solutions. *Chem. Eng. J.* **244**, 202–208.

Hua, M., Zhang, S., Pan, B., Zhang, W., Lv, L. & Zhang, Q. 2012 Heavy metal removal from water/wastewater by nanosized metal oxides: a review. *J. Hazard. Mater.* **211–212**, 317–331.

Hwang, Y., Mines, P. D., Jakobsen, M. H. & Andersen, H. R. 2015 Simple colorimetric assay for dehalogenation reactivity of nanoscale zero-valent iron using 4-chlorophenol. *Appl. Catal. B: Environ.* **166–167**, 18–24.

Jabeen, H., Kemp, K. C. & Chandra, V. 2013 Synthesis of nano zerovalent iron nanoparticles-graphene composite for the treatment of lead contaminated water. *J. Environ. Manage.* **130**, 429–435.

Jiang, M. Q., Jin, X. Y., Lu, X. Q. & Chen, Z. L. 2010 Adsorption of Pb(II), Cd(II), Ni(II) and Cu(II) onto natural kaolinite clay. *Desalination* **252**, 33–39.

Katsoyiannis, A. I. & Zouboulis, I. A. 2002 Removal of arsenic from contaminated water sources by sorption onto iron-oxide-coated polymeric materials. *Water Res.* **36**, 5141–5155.

Kim, S. A., Kamala-Kannan, S., Lee, K. J., Park, Y. J., Shea, P. J., Lee, W. H., Kim, H. M. & Oh, B. T. 2013 Removal of Pb(II) from aqueous solution by a zeolite–nanoscale zero-valent iron composite. *Chem. Eng. J.* **217**, 54–60.

Li, X. Q., Elliott, D. W. & Zhang, W. X. 2006 Zero-valent iron nanoparticles for abatement of environmental pollutants: materials and engineering aspects. *Crit. Rev. Solid State Mater. Sci.* **31**, 111–122.

Li, Z., Dong, H., Zhang, Y., Li, J. & Li, Y. 2017 Enhanced removal of Ni(II) by nanoscale zero valent iron supported on Na-saturated bentonite. *J. Colloid Interface Sci.* **497**, 43–49.

Liu, M., Wang, Y., Chen, L., Zhang, Y. & Lin, Z. 2015 $Mg(OH)_2$ supported nanoscale zero valent iron enhancing the removal of Pb(II) from aqueous solution. *ACS Appl. Mater. Interfaces* **7**, 7961–7969.

Lv, X., Xue, X., Jiang, G., Wu, D., Sheng, T., Zhou, H. & Xu, X. 2014 Nanoscale zero-valent iron (nZVI) assembled on magnetic Fe_3O_4/graphene for chromium (VI) removal from aqueous solution. *J. Colloid Interface Sci.* **417**, 51–59.

Lv, J., An, Q., Zheng, W., Fan, Y., Lei, Z. & Zhai, S. 2016 Multifunctional hierarchical cabbage-like nZVI-Fe_3O_4/C composites for efficient chromium (VI) removal. *J. Taiwan Inst. Chem. E.* **65**, 312–322.

Mackenzie, K., Bleyl, S., Georgi, A. & Kopinke, F. D. 2012 Carbo-iron – an Fe/AC composite – as alternative to nano-iron for groundwater treatment. *Water Res.* **46**, 3817–3826.

Noubactep, C. 2008 A critical review on the process of contaminant removal in Fe^0–H_2O systems. *Environ. Technol.* **29**, 909–920.

Rao, P., Mak, M. S. H., Liu, T. Z., Lai, K. C. K. & Lo, I. M. C. 2009 Effects of humic acid on arsenic (V) removal by zero-valent

Downloaded from http://iwaponline.com/wst/article-pdf/76/10/2680/241237/wst076102680.pdf
by guest

iron from groundwater with special references to corrosion products analyses. *Chemosphere* **75**, 156–162.

Shen, M., Chen, S., Jia, W., Fan, G., Jin, Y. & Liang, H. 2016 Facile synthesis of Ag@Fe_3O_4@C-Au core-shell microspheres for surface-enhanced Raman scattering. *Gold Bull.* **49**, 103–109.

Shi, Y., Huang, J., Wang, J., Su, P. & Yang, Y. 2015 A magnetic nanoscale $Fe_3O_4/P_{\beta\text{-CD}}$ composite as an efficient peroxidase mimetic for glucose detection. *Talanta* **143**, 457–463.

Sun, Y., Ding, C., Cheng, W. & Wang, X. 2014 Simultaneous adsorption and reduction of U(VI) on reduced graphene oxide-supported nanoscale zerovalent iron. *J. Hazard. Mater.* **280**, 399–408.

Üzüm, Ç., Shahwan, T., Eroğlu, A. E., Hallam, K. R., Scott, T. B. & Lieberwirth, I. 2009 Synthesis and characterization of kaolinite-supported zero-valent iron nanoparticles and their application for the removal of aqueous Cu^{2+} and Co^{2+} ions. *Appl. Clay Sci.* **43**, 172–181.

Vijayaraghavan, K. & Joshi, U. M. 2013 Chicken eggshells remove Pb(II) ions from synthetic wastewater. *Environ. Eng. Sci.* **30**, 67–73.

Westerhoff, P. & James, J. 2003 Nitrate removal in zero-valent iron packed columns. *Water Res.* **37**, 1818–1830.

Xi, Y., Mallavarapu, M. & Naidu, R. 2010 Reduction and adsorption of Pb^{2+} in aqueous solution by nano-zero-valent iron-A SEM, TEM and XPS study. *Mater. Res. Bull.* **45**, 1361–1367.

Xu, C. H., Zhu, L. J., Wang, X. H., Lin, S. & Chen, Y. M. 2014 Fast and highly efficient removal of chromate from aqueous solution using nanoscale zero-valent iron/activated carbon (NZVI/AC). *Water, Air, Soil Pollut.* **225**, 1–13.

Yan, W., Lien, H. L., Koel, B. E. & Zhang, W. X. 2013 Iron nanoparticles for environmental clean-up: recent developments and future outlook. *Environ. Sci. Processes & Impacts* **15**, 63–77.

Yang, K., Peng, H. B., Wen, Y. H. & Li, N. 2010 Re-examination of characteristic FTIR spectrum of secondary layer in bilayer oleic acid-coated fe_3o_4 nanoparticles. *Appl. Surf. Sci.* **256**, 3093–3097.

Yang, J., Chen, H., Gao, J., Yan, T., Zhou, F., Cui, S. & Bi, W. 2016 Synthesis of Fe_3O_4/g-C_3N_4 nanocomposites and their application in the photodegradation of 2,4,6-trichlorophenol under visible light. *Mater. Lett.* **164**, 183–189.

Yuan, Y., Li, H., Lai, B., Yang, P., Gou, M., Zhou, Y. & Sun, G. 2014 Removal of high-concentration C.I. acid orange 7 from aqueous solution by zerovalent iron/copper (Fe/Cu) bimetallic particles. *Ind. Eng. Chem. Res.* **53**, 2605–2613.

Zhang, X., Lin, S., Lu, X. Q. & Chen, Z. L. 2010 Removal of Pb(II) from water using synthesized kaolin supported nanoscale zero-valent iron. *Chem. Eng. J.* **163**, 243–248.

Zhang, X., Lin, S., Chen, Z., Megharaj, M. & Naidu, R. 2011 Kaolinite-supported nanoscale zero-valent iron for removal of Pb^{2+} from aqueous solution: reactivity, characterization and mechanism. *Water Res.* **45**, 3481–3488.

Zhang, J., Zhai, S., Li, S., Xiao, Z., Song, Y., An, Q. & Tian, G. 2013 Pb(II) removal of Fe_3O_4@SiO_2–NH_2 core–shell nanomaterials prepared via a controllable sol–gel process. *Chem. Eng. J.* **215–216**, 461–471.

Zhang, Y., Li, Y., Dai, C., Zhou, X. & Zhang, W. 2014 Sequestration of Cd(II) with nanoscale zero-valent iron (nZVI): characterization and test in a two-stage system. *Chem. Eng. J.* **244**, 218–226.

First received 27 February 2017; accepted in revised form 16 June 2017. Available online 28 July 2017

Downloaded from http://iwaponline.com/wst/article-pdf/76/10/2680/241237/wst076102680.pdf
by guest